ISSN 2250-3153

Geotechnical Soil Characterization of Akanfa–Gbaran Road, Bayelsa State, Nigeria

Ngerebara Owajiokiche Dago[+], Abam T. K. S[+] and Nelson Kiri[*]

[+]Geotechnics Division, Institute of Geosciences and Space Technology, Rivers State University of Science and Technology, PMB 5080, PortHarcourt, Nigeria.
[*]Groundscan Services Nigeria Limited, 5 Harold Wilson Drive, P.O.Box 9528, PortHarcourt, Nigeria

Abstract- The Akanfa–Gbaran Road traverses sections of the geomorphic meander belt and crosses the Epie Creek, near Yenegoa, Bayelsa State capital. Road construction in this area is usually at exceptionally high cost because of the challenging geologic, geomorphic and environmental setting of the Niger delta. Using a combination of geotechnical borings and Cone penetration soundings, the subgrade underlying the road was characterized, providing litho-stratigraphic, shear strength, bearing capacity, settlement and axial pile capacity data for the area. Results show that competent bearing soil layers occur at shallow depths and only the top 1.5m of the subgrade need be improved for effective pavement performance. Predicted axial pile capacities for a range of closed ended, steel tubular pile diameters 300mm, 450mm and 600mm show that pile embedment need not exceed 15m except for considerations of scour.

Index Terms- Sub-grade, Pile load, Stratigraphy, California Bearing Ratio (CBR), Bridge Abutment, Cone Penetrometer Test (CPT), Standard Penetration Test (SPT)

I. INTRODUCTION

Bayelsa State was established in 1996 at a time when the Federal presence was a mere 30km road connecting Mbiama to Yenagoa. A commonly advanced reason for the lack of physical infrastructure was difficult terrain, occasioned by challenging geologic, geomorphic and environmental setting of the Niger Delta region. Overcoming the constraint to development of difficult terrain was indeed overwhelming reason for the creation of a number of specialized agencies of government such as OMPADEC, NDDC, NDBDA and indeed Bayelsa State itself. The dare absence of road infrastructure matched against the desire for rapid transformation of the state demanded investments in the expansion of the transport sector. This necessitated the construction of the Akanfa to Gbaran road with a bridge link spanning about 150m (figure 1). The underlying soils along the road alignment and across the adjoining river were evaluated in order to characterize the subgrade for the design of suitable pavement and bridge foundation for each of the piers.

Sub-grades play an important role in imparting structural stability to the pavement structure as it receives loads imposed upon it by road traffic. Traffic loads need to be transmitted in a manner that the subgrade-deformation is within elastic limits, and the shear forces developed is within safe limits under adverse climatic and loading conditions. The sub-grade in the locality comprises unbound earth materials such as sand, silt and clay that influence the design and construction of roads. The assessment of properties of soil sub-grades, in terms of density, soil stiffness, strength, and other in-situ parameters is vital in the design of roads, and their performance.

Traditionally, flexible pavements are designed based on the CBR approach or by considering elastic deformations. The CBR approach to pavement design gained popularity among practicing engineers in the late 1980s with the use of advanced computing power and speed (Rollings 2003).This approach to flexible pavement design gives more importance to the estimation of the density of the sub-grades and the pavement layers. Other design philosophies for flexible pavement do exist, including those with more of a basis in the theory of the mechanics of materials-such as layered elastic and finite element approaches. In the classical approach to design of flexible pavements using the Burmister's (1958) layer theory, estimate of the elastic modulus of the sub-grade is necessary to determine the required layer-thickness of a pavement structure.

Despite the advances in these state-of-the art approaches to pavement design, the CBR approach continues to be one of the most reliable methods for pavement design, especially in the design of pavements for military and civilian aviation (Semen 2006).

According to Chen et al. (1999), Livneh and Goldberg (2001), although 'density' is a good indicator of the strength of granular sub-grades, it is also necessary to investigate the modulus of the sub-grade, since these measures represent different natural characteristics.

Fig.1: Map of the Niger Delta showing the project area.

Pavement evaluation and design analysis relies mainly on information on the stiffness of pavement layers and the modulus of sub-grades as references, in addition to supplementary data on density and moisture content (Huang, 2004). It is often required to estimate the sub-grade-stiffness or modulus of the pavements, before and after their construction as part of the quality-control measures, and also for quality assurance (Chen et al., 2005).

Al-Amoudi *et al* (2002) and the Bureau of Indian Standards for soil tests and determination of CBR noted that some simpler and faster methods of pavement evaluation can correlate very well with CBR test. Also, according to the manufacturers of non-destructive testing equipment, the relationships between the CBR values and the moduli of elasticity are dependent upon the local geology (Phillips 2005).

The use of dynamic cone penetrometers (DCP) was applied in the evaluation of sub- grades based on the resistance offered to penetration according to De Beer, (1990) and Rahim *et al* (2002). In this way, the traditional approaches of CBR and DCP were correlated with modulus of elasticity to influence judgement on the sub-grade characteristics in the area. Earlier, Ngerebara *et al* (2012) had looked at the influence of ground water saturation on the sub-grade shear strength and modulus to withstand stress imposed by the axle load in parts of the area.

II. Geology and Site Description

The development of a delta is governed by the interactions of the processes of subsidence, deposition and erosion (Sullivan and Squire, 1980). These interactions create complex sequences of interbeded sands, silts, clays and organic rich sediments termed lithofacies. The sediments which form the delta also vary with distance from sediment source. The more proximal deposition zones, such as the shoreline, are dominated by tidal channel and coastal barrier sands overlaying earlier (Holocene) marine clays (NDES, 1999). The delta slope deposition zone, in water depths of approximately 15m, is characterized by marine sands.

The local geology around the Akanfa is composed of sediments which are characteristic of several depositional environments. The general geology of the area essentially reflects the influence of movements of rivers, in the Niger delta and their search for lines of flow to the sea with consequent deposition of transported sediments. The surface deposits in this area comprises silty and sandy-clays. The sandy layers underlying the silty-sandy clay are predominantly medium to coarse in grain sizes and found to exist in mostly medium state of compaction.

III. Methods of Investigation

The field investigations involved the drilling of five (5No) boreholes to a depth of 30m at the bridge abutments and along the river crossing. This was augmented by five auger borings made at intervals of 100m along the proposed road alignment on both sides of the bridge. In addition, five (5No) Cone Penetration Tests (CPT) were carried out at each auger boring location along the proposed alignment to provide additional information on bearing capacity, CBR and compressibility characteristics of the sediments along the alignment.

The geotechnical bores were made using the light shell and auger motorized percussion rig with undisturbed cohesive soil sampling and in-situ Standard Penetration testing resulting in the determination of SPT-N values for the cohesionless sediment layers. Standard Penetration Tests (SPT) were performed every 1.5m advance through cohesionless soils. The main objective of this test is to assess the relative densities of the cohesionless soils penetrated. The hydraulically operated GMF type of static

penetrometer having 100KN capacity was used for cone resistance soundings.

IV. Results and Discussions

The composite lithologs of the boreholes across the site is presented in Figure 2, showing the stratigraphy and layered structure of the sediments beneath the road and bridge alignment. The penetration resistance profiles in blow counts with depth are indicated on the composite logs to indicate the relative strengths of the respective soil layers. In addition, the cone resistance profile for the top 5m in the pavement sections of the road are presented in Figure3. Using the CPT data, undrained strength values and depth profiles were derived along with the California Bearing Ratio (CBR) as presented in Figure 3.

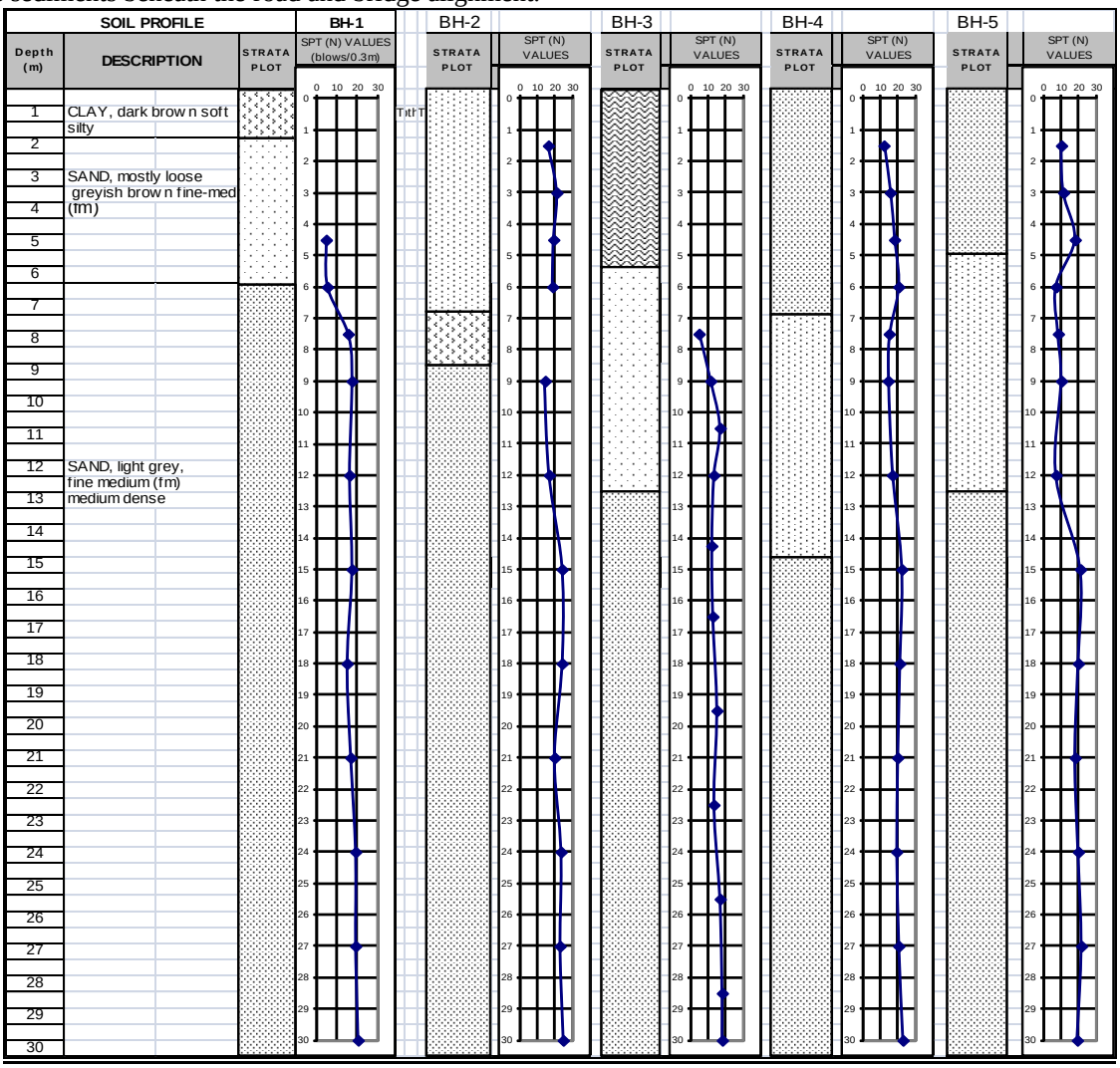

Figure 2: Composite litho-stratigraphy underlying the Akanfa–Gbaran Road

Bearing Capacity Computations and Analysis

The bearing capacity analysis for the underlying soils was limited to the near surface silty clay soil since the induced traffic load would hardly extend beyond it. The ultimate net bearing capacity (qn) of a shallow foundation was calculated using the basic relationship:

(for strip) $q_{nu} = CN_c + P_o (N_q) + 0.5\gamma BN_\gamma$
(for square or Rectangular foundation) $q_{nu} = 1.2CN_c (1 + 0.3B/L) + P_o (N_q) + 0.5\gamma BN_\gamma (1– 0.2B/L)$

where: γ = the bulk density of the soil below the foundation level
C = the undrained shear strength of the soil
P_o is the effective overburden pressure at the foundation level

N_c, N_q, N_γ = Terzaghi's bearing capacity factors obtained from charts

An alternative approach was adopted for quality control purposes in which the derived undrained strength values from the CPT were used for the direct estimation of the bearing capacity using the well established equation:

$$Cu = q_c - \sigma^1_{vo}/N_k$$

Where

$qc - \sigma^1_{vo}$ = net cone resistance

N_k = Cone factor

Using combinations of these relationships, the ultimate bearing and safe pressures were obtained for various foundation depths (Figures 3a-3b).

	CPT-1	Undrained	Ultimate Bearing	Allowable Bearing
Depth (m)	(kg/cm^2)	Strength (kPa)	(kPa)	Safe Bearing Pressure (kPa)
0.2	4	19.82	116.57	38.86
0.4	4	19.64	119.15	39.72
0.6	4	19.46	121.72	40.57
0.8	10	49.28	295.30	98.43
1	8	39.10	240.87	80.29
1.2	10	48.92	300.44	100.15
1.4	10	48.74	303.02	101.01
1.6	12	58.56	362.59	120.86
1.8	6	28.38	194.17	64.72
2	10	48.20	310.74	103.58
2.2	25	123.02	740.81	246.94
2.4	50	247.84	1455.89	485.30
2.6	55	272.66	1600.96	533.65
2.8	60	297.48	1746.04	582.01
3	65	322.30	1891.11	630.37
3.2	68	337.12	1979.18	659.73
3.4	75	371.94	2181.26	727.09
3.6	85	421.76	2468.83	822.94
3.8	90	446.58	2613.91	871.30
4	100	496.40	2901.48	967.16
4.2	115	571.22	3331.55	1110.52
4.4	120	596.04	3476.63	1158.88
4.6	140	695.86	4049.20	1349.73

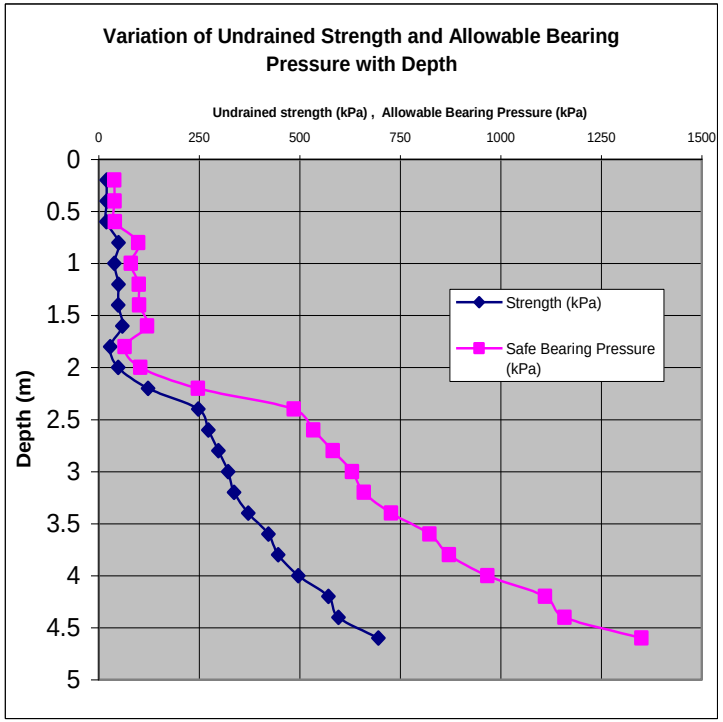

Fig.3a: Undrained strength and Bearing Pressure derived from Cone Penetration Sounding at Point-1

	CPT-2	Undrained	Ultimate Bearing	Allowable Bearing
Depth (m)	(kg/cm^2)	Strength (kPa)	(kPa)	(kPa)
0.2	2	9.82	59.57	19.86
0.4	2	9.64	62.15	20.72
0.6	3	14.46	93.22	31.07
0.8	2	9.28	67.30	22.43
1	4	19.10	126.87	42.29
1.2	6	28.92	186.44	62.15
1.4	10	48.74	303.02	101.01
1.6	11	53.56	334.09	111.36
1.8	9	43.38	279.67	93.22
2	10	48.20	310.74	103.58
2.2	10	48.02	313.31	104.44
2.4	10	47.84	315.89	105.30
2.6	12	57.66	375.46	125.15
2.8	12	57.48	378.04	126.01
3	12	57.30	380.61	126.87
3.2	8	37.12	269.18	89.73
3.4	9	41.94	300.26	100.09
3.6	10	46.76	331.33	110.44
3.8	10	46.58	333.91	111.30
4	10	46.40	336.48	112.16
4.2	10	46.22	339.05	113.02
4.4	8	36.04	284.63	94.88
4.6	6	25.86	230.20	76.73
4.8	6	25.68	232.78	77.59
5	6	25.50	235.35	78.45
5.2	8	35.32	294.92	98.31
5.4	10	45.14	354.50	118.17
5.6	14	64.96	471.07	157.02
5.8	40	194.78	1214.65	404.88
6	120	594.60	3497.22	1165.74

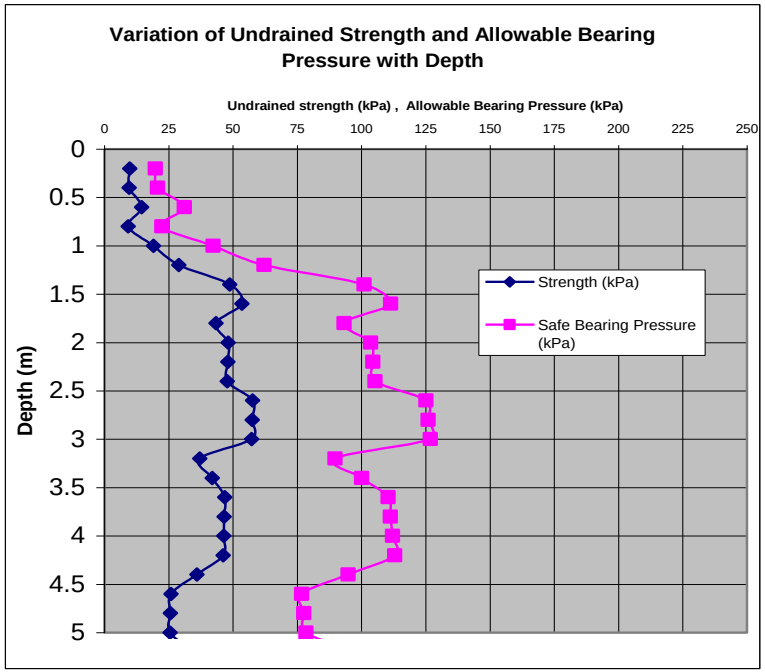

Fig.3b: Undrained strength and Pressure derived from Cone Penetration Sounding at Point-2

	CPT-3	Undrained	Ultimate Bearing	Allowable Bearing
Depth (m)	(kg/cm^2)	Strength (kPa)	(kPa)	(kPa)
0.2	4	19.82	116.57	38.86
0.4	4	19.64	119.15	39.72
0.6	4	19.46	121.72	40.57
0.8	3	14.28	95.80	31.93
1	2	9.10	69.87	23.29
1.2	4	18.92	129.44	43.15
1.4	6	28.74	189.02	63.01
1.6	8	38.56	248.59	82.86
1.8	9	43.38	279.67	93.22
2	12	58.20	367.74	122.58
2.2	20	98.02	598.31	199.44
2.4	25	122.84	743.39	247.80
2.6	32	157.66	945.46	315.15
2.8	18	87.48	549.04	183.01
3	8	37.30	266.61	88.87
3.2	6	27.12	212.18	70.73
3.4	4	16.94	157.76	52.59
3.6	6	26.76	217.33	72.44
3.8	6	26.58	219.91	73.30
4	6	26.40	222.48	74.16
4.2	6	26.22	225.05	75.02
4.4	8	36.04	284.63	94.88
4.6	12	55.86	401.20	133.73
4.8	12	55.68	403.78	134.59
5	16	75.50	520.35	173.45
5.2	16	75.32	522.92	174.31
5.4	18	85.14	582.50	194.17
5.6	21	99.96	670.57	223.52
5.8	32	154.78	986.65	328.88
6	24	114.60	761.22	253.74
6.2	16	74.42	535.79	178.60
6.4	12	54.24	424.37	141.46
6.6	8	34.06	312.94	104.31
6.8	80	393.88	2367.52	789.17
7	90	443.70	2655.09	885.03
7.2	115	568.52	3370.16	1123.39

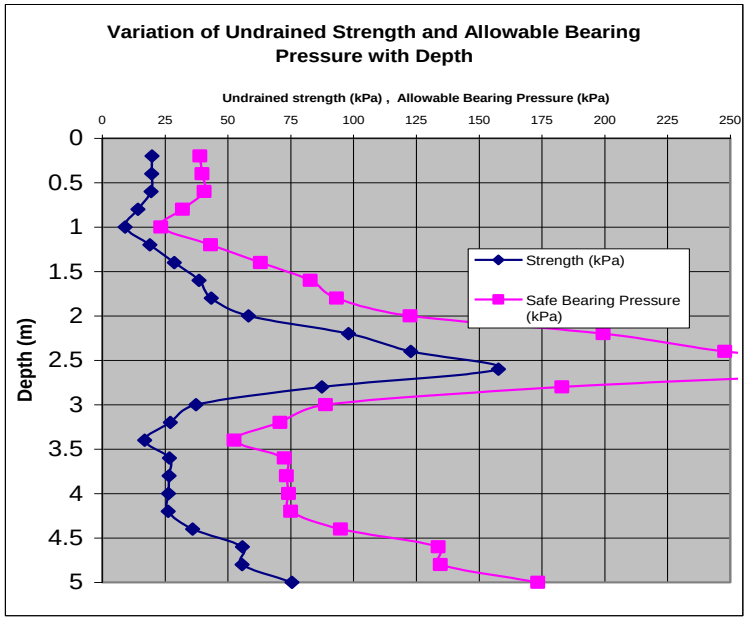

Fig.3c: Undrained strength and Pressure derived from Cone Penetration Sounding at Point-3

Depth (m)	CPT-4 (kg/cm^2)	Undrained Strength (kPa)	Ultimate Bearing (kPa)	Allowable Bearing (kPa)
0.2	3	14.82	88.07	29.36
0.4	4	19.64	119.15	39.72
0.6	4	19.46	121.72	40.57
0.8	3	14.28	95.80	31.93
1	3	14.10	98.37	32.79
1.2	4	18.92	129.44	43.15
1.4	5	23.74	160.52	53.51
1.6	6	28.56	191.59	63.86
1.8	8	38.38	251.17	83.72
2	11	53.20	339.24	113.08
2.2	18	88.02	541.31	180.44
2.4	25	122.84	743.39	247.80
2.6	30	147.66	888.46	296.15
2.8	14	67.48	435.04	145.01
3	8	37.30	266.61	88.87
3.2	5	22.12	183.68	61.23
3.4	5	21.94	186.26	62.09
3.6	5	21.76	188.83	62.94
3.8	6	26.58	219.91	73.30
4	6	26.40	222.48	74.16
4.2	7	31.22	253.55	84.52
4.4	7	31.04	256.13	85.38
4.6	12	55.86	401.20	133.73
4.8	13	60.68	432.28	144.09
5	17	80.50	548.85	182.95
5.2	17	80.32	551.42	183.81
5.4	17	80.14	554.00	184.67
5.6	20	94.96	642.07	214.02
5.8	31	149.78	958.15	319.38
6	24	114.60	761.22	253.74
6.2	16	74.42	535.79	178.60
6.4	14	64.24	481.37	160.46
6.6	9	39.06	341.44	113.81
6.8	60	293.88	1797.52	599.17
7	85	418.70	2512.59	837.53
7.2	89	438.52	2629.16	876.39
7.4	105	518.34	3087.74	1029.25
7.6	120	593.16	3517.81	1172.60

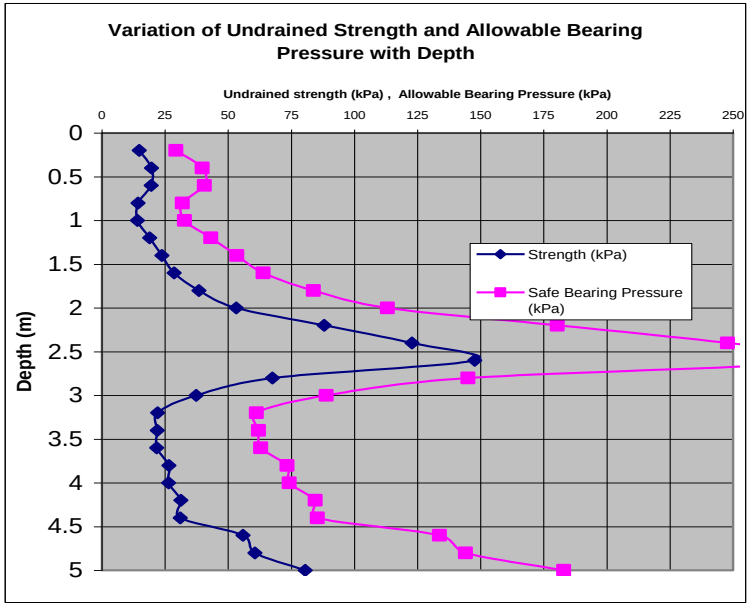

Fig.3d: Undrained strength and Pressure derived from Cone Penetration Sounding at Point-4

	CPT-5	Undrained	Ultimate Bearing	Allowable Bearing
Depth (m)	(kg/cm^2)	Strength (kPa)	(kPa)	(kPa)
0.2	3	14.82	88.07	29.36
0.4	4	19.64	119.15	39.72
0.6	4	19.46	121.72	40.57
0.8	4	19.28	124.30	41.43
1	3	14.10	98.37	32.79
1.2	4	18.92	129.44	43.15
1.4	5	23.74	160.52	53.51
1.6	5	23.56	163.09	54.36
1.8	6	28.38	194.17	64.72
2	8	38.20	253.74	84.58
2.2	18	88.02	541.31	180.44
2.4	22	107.84	657.89	219.30
2.6	30	147.66	888.46	296.15
2.8	18	87.48	549.04	183.01
3	8	37.30	266.61	88.87
3.2	6	27.12	212.18	70.73
3.4	5	21.94	186.26	62.09
3.6	6	26.76	217.33	72.44
3.8	6	26.58	219.91	73.30
4	6	26.40	222.48	74.16
4.2	6	26.22	225.05	75.02
4.4	7	31.04	256.13	85.38
4.6	13	60.86	429.70	143.23
4.8	12	55.68	403.78	134.59
5	15	70.50	491.85	163.95
5.2	16	75.32	522.92	174.31
5.4	17	80.14	554.00	184.67
5.6	20	94.96	642.07	214.02
5.8	32	154.78	986.65	328.88
6	25	119.60	789.72	263.24
6.2	16	74.42	535.79	178.60
6.4	12	54.24	424.37	141.46
6.6	8	34.06	312.94	104.31
6.8	15	68.88	515.02	171.67
7	75	368.70	2227.59	742.53
7.2	120	593.52	3512.66	1170.89

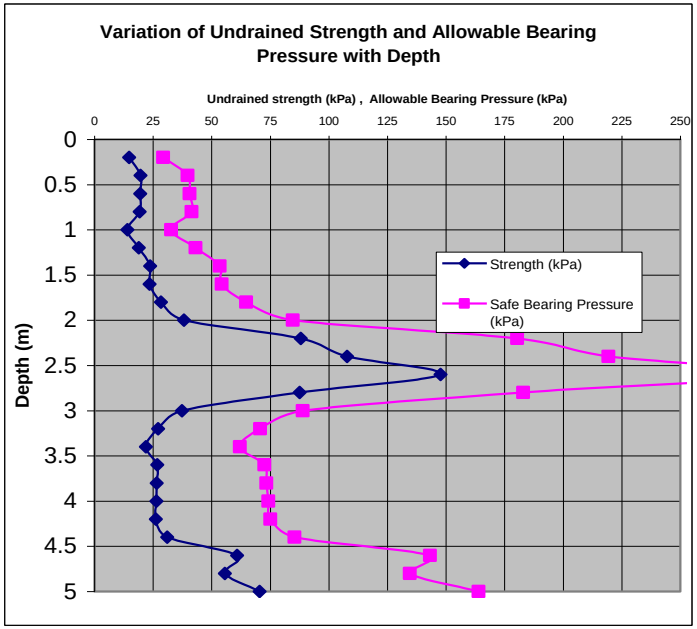

Fig.3e: Undrained strength and Pressure derived from Cone Penetration Sounding at Point-5

V. PILED FOUNDATION

The geotechnical data across the river was further analyzed to determine axial pile capacities at various depths in the underlying soil formation. Ultimate Pile capacity for axial loading was estimated for driven, single, straight-shafted, close-ended, tubular steel pile 300mm, 450mm and 600mm in diameter using API or conventional method. This method, which is currently the most widely applied, uses the results of the laboratory tests on soil sample and the blow counts from standard penetration tests in the prediction of the ultimate axial pile capacity as follows:

(i) Ultimate base resistance in clay

$$\mathbf{Q_{bs} = 9.c_u.A_b}$$

(ii) Ultimate base resistance in sand

$$\mathbf{Q_{bs} = P^1_0.N_q.A_b.}$$

(iii) Ultimate shaft resistance in clay

$$\mathbf{Q_{sc} = \alpha\, c_u.A_s}$$

(iv) Ultimate shaft resistance in sand

$$\mathbf{Q_{ss} = K_s.P_0.\tan\delta.A_s}$$

C_u = average undrained cohesion at the pile base
A_b = base area of the pile
P_0 = effective overburden pressure at the pile base
N_q = bearing capacity factor
A_s = exposed area of shaft
K_s= coefficient of lateral earth pressure (K_s/K_0 = 1 to 2), for small displacement piles ratio varies from 0.75 to 1.75, K_0 = 0.6
P_0 = average effective overburden pressure over soil layer
α= pile wall adhesion
δ = effective soil/pile friction angle (smooth surface = 0.5 ϕ to 0.7ϕ)
Undrained strength to which a factor of safety of 1.8 has been applied as recommended by Eurocode, $C_{ub} = \underline{Cu}$
(Fs = 1.5 – 1.8)

Ultimate carrying capacity $Q_{ult} = Q_b + Q_s$
Allowable $Q_a = \underline{Q_b + Q_s}$
3

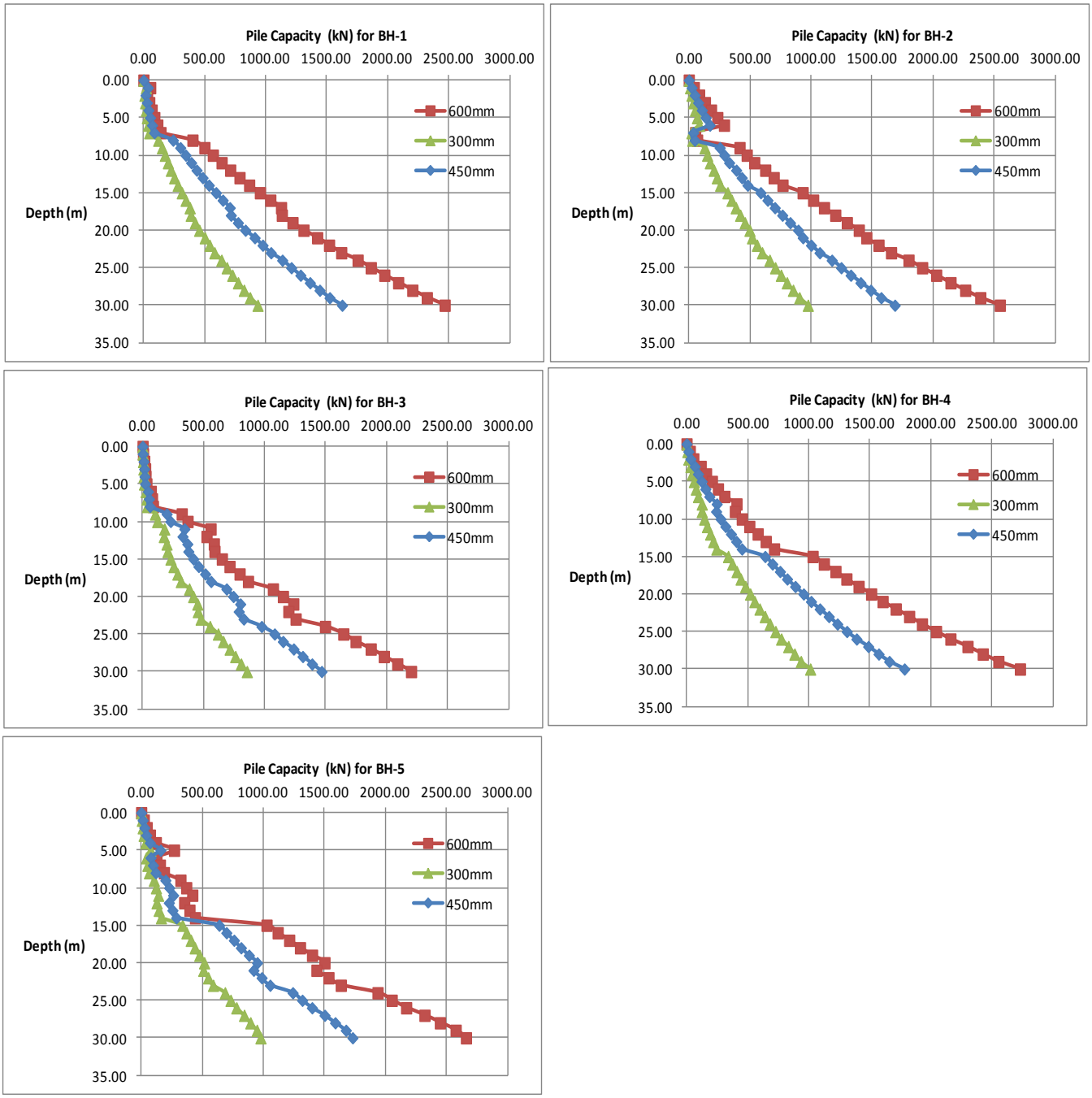

Fig.4: Predicted Axial Pile Capacities for various diameters of driven, closed ended, steel tubular piles.

VI. CONCLUSIONS

Stratigraphy across the site shows layered structure of the sediments beneath the road and bridge alignments. The penetration resistance profiles with depth gives an indication of the relative strengths of the respective soil layers. Using the CPT data, undrained strength and bearing pressure values were derived along with the California Bearing Ratio (CBR) and this is limited to the near surface silty clay soil since the induced traffic load would hardly extend beyond it.

Ultimate Pile capacity for axial loading was estimated for driven, single, straight-shafted, close-ended, tubular steel pile 300mm, 450mm and 600mm diameter at 15m depth, using combined results of the laboratory tests on soil sample and the blow counts from standard penetration tests in the prediction of the ultimate axial pile capacity.

Given the appropriate design thickness of sub-base, base, and pavement as determined by the CBR design values for each of the materials, there is no doubt that the road will last for the normal duration of such flexible pavement.

REFERENCES

[1] Al-Amodi, O. S. B., Asi, I. M., Al-Abdul Wahab, H. I., and Khan, Z.. A. 2002. Clegg hammer-California bearing ratio correlations.Journal of Materials in Civil Engineering ASCE. 512-523.

[2] Burmister, D. M. 1958. Evaluation of Pavement Systems of the WASHO Road Test by Layer System Method, Highway Research Board Bulletin 177, 26-54.

[3] Chen, Dar-Hao., Wu, Wei., He, Rong., Bilyeu, John., Arrelano, Mike. 1999. Evaluation of in-situ resilient modulus testing techniques, in Proc. Transportation Research Board Annual Meeting.

[4] Chen, D. H., Wang, J. N., and Bilyeu, J. 2001. Application of Dynamic Cone Penetrometer in evaluation of base and subgrade layers, Transp. Res. Rec. 1764 (Transportation Research Board: Washington, DC).

[5] Chen, D. H., Lin, D. F., Pen-Hwang Liau, P. H., and Bilyeu, J. 2005. A correlation between Dynamic Cone Penetrometer values and pavement layer oduli, Geotechnical Testing Journal, 38(1).

[6] Chen, J., Hossain, M., and Latorella, T. M. 1999. Use of Falling Weight Deflectometer and Dynamic Cone Penetrometer in Pavement Evaluation, Transp. Res. Rec. 1655, Trans. Res. Board, 145-151.

[7] De Beer, M. 1990. Use of Dynamic Cone Penetrometer in the design of road structures, Geo-techniques in African Environment, pp. 167-176 (Balkema: Rotterdam).

[8] Huang, Y. H. 2004. Pavement Analysis and Design, Prentice-Hall, Englewood Cliffs, NJ.

[9] Indian Standard Method of Test for Soils (1979), Part 16 Laboratory Determination of CBR, First Revision, Bureau of Indian Standards, Revised in 1989.

[10] Livneh, M. and Goldberg, Y. 2001. Quality Assessment during Road Formation and Foundation Construction: Use of Falling- Weight Deflectometer and Light Drop Weight, Transportation Research Record 1755, TRB, National Research Council, Washington, D.C., 69-77.

[11] Ngerebara, O.D.; Aitsebaomo, F. O; Teme, S. C and Abam, T. K. S (2012): Groundwater Table and California Bearing Ratio Relationship in Pavement Structure along East-West Highway, Rivers State, Nigeria; Journal of Engineering Research, Vol. 17, No. 3

[12] Niger Delta Environmental Survey (NDES) (1999) Physical Environment Report on the Hydrology of the Niger Delta

[13] Phillips, L. D. 2005. Field evaluation of Rapid Airfield Technologies. MS thesis, Mississippi State University, Mississippi State, Mississippi.

[14] Rollings, R. S. 2003. Evaluation of Airfield Design Philosophies. "Proceedings of the 22nd PIARC World Road Congress. Durban, South Africa, 19-25 October. Cedex, France. World Road Association.

[15] Rahim, A. M., and George, K. P. 2002. Automated Dynamic Cone Penetrometer for subgrade resilient modulus characterization, in Proc. 81st Annual Meeting Transportation Board.

[16] Semen, P. M. 2006. A Generalized Approach to Soil Strength Prediction with Machine Learning Methods, US Army Corps of Engineers, Engineer Research and Development Centre.

AUTHORS

First Author- Dr. Ngerebara Owajiokiche Dago, B.Sc, PGD, M.Phil, Ph.D, Institute of Geosciences and Space Technology (IGST), Rivers State University of Science and Technology, Port Harcourt, Nigeria

Second Author- Prof. T. K. S. Abam, B.Sc, M.Sc, M.Sc, Ph.D, Institute of Geosciences and Space Technology (IGST), Rivers State University of Science and Technology, Port Harcourt, Nigeria

Third Author- Nelson Kiri, Groundscan Services Nigeria Limited, 5 Harold Wilson Drive, Port Harcourt, Nigeria

Corresponding Author- Dr. Ngerebara Owajiokiche Dago, Email: n_dago@yahoo.com, Phone number-23408028462055

Table 1: Average Properties for soil under 2m below ground level

Auger Boring	Ultimate Bearing Capacity (kN/m^2)	Allowable Bearing Capacity (kN/m^2)	Coefficient of Sub-grade Reaction (kN/m^3)	Max. Dry Density (kg/m^3)	Optimum Moisture (%)	CBR	
						Unsoaked	Soaked
AG-BH1	236.5	78.8	9458	1.59	19	8	3
AG-BH2	182.3	60.8	7292	1.615	18	9.5	4.2
AG-BH3	173.8	57.9	6950	1.59	19.2	8.5	3.5
AG-BH4	159.5	53.2	6380	1.51	20.2	8.7	3.6
AG-BH5	145.3	48.0	5810	1.59	20.7	10	4

Table 2: Cohesive Soil Index Properties

BH No.	Depth (m)	Moisture	Liquid	Plastic	Plasticity	Liquidity	% Fines	Activity	Compressibility	Swell	Coeff of
		Content (%)	Limit (%)	Limit (%)	Index (%)	Index	<2microns	(Ac)	(Cc)	Potential	Earth Pressure (Ko)
1	0.75	27.1	47	19.9	27.1	0.27	30	0.90	0.333	6.77	0.55
3	0.75	25.5	47.8	24.3	23.5	0.05	38	0.62	0.3402	4.78	0.54
	1.5	21.5	53	18	35	0.10	42	0.83	0.387	12.65	0.59
	5.25	33.7	58	20.4	37.6	0.35	38.5	0.98	0.432	15.06	0.60

Table 3: Strength Related Soil Properties

BH No.	Depth (m)	Moisture	Bulk Unit	Dry Unit	Undrained	Ang. Of Friction	Coeff of	Shear	Strength	Strength
		Content (%)	Wt (kN/m^3)	Wt (kN/m^3)	Cohesion (kPa)	(Deg.)	Earth Pressure (Ko)	Modulus (Es) MPa	Torvane ((kPa)	Pocket Pen ((kPa)
1	0.75	27.1	18.3	14.40	25	3	0.90	18.75	26.5	24
3	0.75	25.5	16.2	12.91	15	2.8	0.90	11.25	26	25
	1.5	21.5	17.4	14.32	37	6	0.85	27.75	29.4	30
	5.25	33.7	15.6	11.67	34	5	0.86	25.5	33.4	32

Table 4: Dynamic soil Properties

BH No.	Depth (m)	SPT(N)	Ncor	Shear Velocity (m/s)	Bulk Unit Wt (kN/m^3)	Relative Density (Dr)	Ang. Of Friction (Deg.)	Dynamic Modulus (G')	Coeff of Earth Pressure (Ko)	Shear Modulus (Es) kPa
1	4.5	8	5	138.23	16.76	30.62	29.80	36.30	0.45	4950.0
	6	9	5	143.37	16.69	31.24	30.39	39.05	0.44	5100.0
	7.5	26	16	199.20	17.72	49.20	37.66	75.39	0.34	7650.0
	9	29	17	206.06	17.72	50.62	38.65	80.67	0.33	8100.0
	12	27	16	201.54	17.43	47.41	38.00	77.18	0.33	7800.0
	15	29	17	206.06	17.36	47.72	38.65	80.67	0.33	8100.0
	18	25	15	196.79	17.07	43.70	37.32	73.58	0.34	7500.0
	21	28	17	203.83	17.08	45.19	38.33	78.94	0.33	7950.0
	24	32	19	212.44	17.14	47.27	39.60	85.75	0.31	8550.0
	27	32	19	212.44	17.06	46.63	39.60	85.75	0.31	8550.0
	30	34	20	216.47	17.05	47.35	40.20	89.04	0.30	8850.0
2	1.5	27	16	201.54	18.89	60.26	38.00	77.18	0.33	7800.0
	3	35	21	218.43	18.69	62.56	40.49	90.65	0.30	9000.0
	4.5	32	19	212.44	18.31	57.33	39.60	85.75	0.31	8550.0
	6	31	19	210.36	18.07	54.66	39.29	84.08	0.32	8400.0
	9	24	14	194.32	17.50	46.46	36.97	71.74	0.35	7350.0
	12	28	17	203.83	17.48	48.19	38.33	78.94	0.33	7950.0
	15	40	24	227.66	17.72	55.19	41.91	98.47	0.28	9750.0
	18	40	24	227.66	17.59	54.05	41.91	98.47	0.28	9750.0
	21	33	20	214.48	17.27	48.67	39.90	87.40	0.31	8700.0
	24	39	23	225.88	17.36	51.69	41.63	96.94	0.29	9600.0
	27	38	23	224.07	17.25	50.40	41.35	95.39	0.29	9450.0
	30	41	25	229.41	17.26	51.53	42.18	99.99	0.28	9900.0
3	7.5	8	5	138.23	16.40	28.87	29.80	36.30	0.45	4950.0
	9	19	11	180.74	17.24	41.80	35.10	62.07	0.38	6600.0
	10.5	28	17	203.83	17.57	48.94	38.33	78.94	0.33	7950.0
	12	22	13	189.15	17.21	43.21	36.25	67.97	0.36	7050.0
	14.25	20	12	183.64	16.98	40.58	35.49	64.07	0.37	6750.0
	16.5	21	13	186.44	16.93	40.79	35.87	66.04	0.36	6900.0
	19.5	25	15	196.79	17.01	43.30	37.32	73.58	0.34	7500.0
	22.5	22	13	189.15	16.77	40.20	36.25	67.97	0.36	7050.0
	25.5	28	17	203.83	16.95	44.19	38.33	78.94	0.33	7950.0
	28.5	30	18	208.23	16.95	45.01	38.97	82.39	0.32	8250.0
	30	30	18	208.23	16.91	44.74	38.97	82.39	0.32	8250.0

Table 4: Dynamic soil Properties Cont'd

BH No.	Depth (m)	SPT(N)	Ncor	Shear Velocity (m/s)	Bulk Unit Wt (kN/m^3)	Relative Density (Dr)	Ang. Of Friction (Deg.)	Dynamic Modulus (G')	Coeff of Earth Pressure (Ko)	Shear Modulus (Es) kPa
4	1.5	20	12	183.64	18.55	52.60	35.49	64.07	0.37	6750.0
	3	26	16	199.20	18.36	54.68	37.66	75.39	0.34	7650.0
	4.5	30	18	208.23	18.24	55.68	38.97	82.39	0.32	8250.0
	6	34	20	216.47	18.18	57.00	40.20	89.04	0.30	8850.0
	7.5	25	15	196.79	17.68	48.33	37.32	73.58	0.34	7500.0
	9	24	14	194.32	17.50	46.46	36.97	71.74	0.35	7350.0
	12	28	17	203.83	17.48	48.19	38.33	78.94	0.33	7950.0
	15	37	22	222.22	17.63	53.28	41.07	93.83	0.29	9300.0
	18	35	21	218.43	17.44	50.88	40.49	90.65	0.30	9000.0
	21	33	20	214.48	17.27	48.67	39.90	87.40	0.31	8700.0
	24	32	19	212.44	17.14	47.27	39.60	85.75	0.31	8550.0
	27	34	20	216.47	17.13	47.93	40.20	89.04	0.30	8850.0
	30	38	23	224.07	17.18	49.79	41.35	95.39	0.29	9450.0
5	1.5	17	10	174.62	18.37	48.87	34.28	57.93	0.39	6300.0
	3	19	11	180.74	18.01	47.45	35.10	62.07	0.38	6600.0
	4.5	30	18	208.23	18.24	55.68	38.97	82.39	0.32	8250.0
	6	12	7	156.74	17.01	35.58	32.00	46.68	0.42	5550.0
	7.5	14	8	164.42	17.03	37.18	32.96	51.36	0.41	5850.0
	9	17	10	174.62	17.12	39.75	34.28	57.93	0.39	6300.0
	12	12	7	156.74	16.53	32.86	32.00	46.68	0.42	5550.0
	15	35	21	218.43	17.57	51.96	40.49	90.65	0.30	9000.0
	18	33	20	214.48	17.38	49.54	39.90	87.40	0.31	8700.0
	21	30	18	208.23	17.16	46.62	38.97	82.39	0.32	8250.0
	24	33	20	214.48	17.17	47.93	39.90	87.40	0.31	8700.0
	27	36	22	220.34	17.19	49.18	40.78	92.25	0.30	9150.0
	30	32	19	212.44	16.98	46.07	39.60	85.75	0.31	8550.0

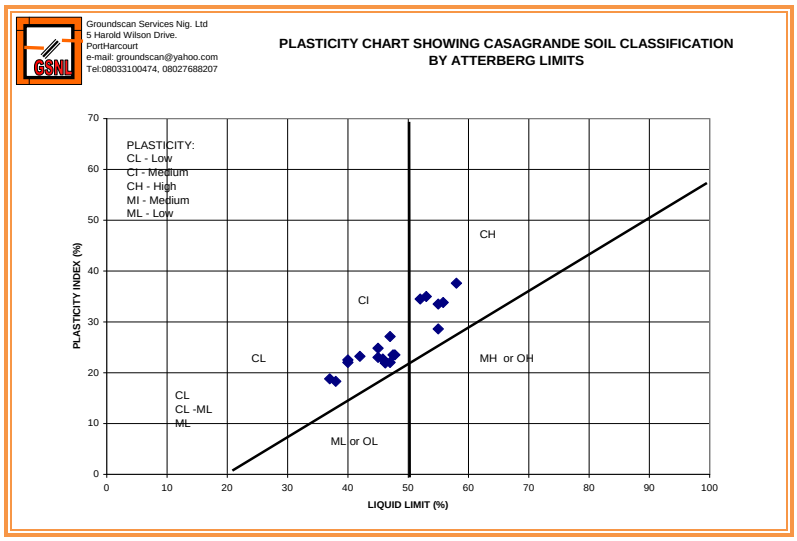

Figure 4: Soil Classification by Atterberg Limits